

Elastic collisions and rotational excitation in positron scattering from CO₂ molecules

F. A. Gianturco* and P. Paoletti

Department of Chemistry, The University of Rome, Città Universitaria, 00185 Rome, Italy

(Received 25 June 1996)

Full quantum calculations are carried out for the elastic (rotationally summed) integral and differential cross sections in low-energy collisions of positrons with rigid rotor CO₂ molecules. The interaction includes an expansion of the exact Coulomb potential on a single-center (SCE) and a parameter-free correlation-polarization (V_{CP}) potential given in local form via density-functional theory (DFT) with gradient corrections. State-to-state rotationally inelastic cross sections (integral and differential) are also presented and their behavior is discussed in relation to what is known from similar experiments with electrons as projectiles. The agreement found between computed and measured elastic integral cross sections is rather good and confirms the realistic quality of a DFT treatment for short-range dynamical correlation effects.

[S1050-2947(97)05703-X]

PACS number(s): 34.90.+q, 34.10.+x

I. INTRODUCTION

The low-energy scattering processes involving positrons as projectiles and simple molecular targets in the gas phase have gained a great deal of importance in the last ten years or so because of the various areas of chemistry and physics where they are considered to be relevant [1,2]. The variety of processes for which such projectiles are studied parallel that for electron collisions with molecular targets, where elastic scattering excitations of molecular degrees of freedom, reactions that alter the final nature of the molecular targets have been observed in increasingly greater detail [3]. In addition, the possibility of positronium (Ps) formation into various excited states presents both experiments and theoretical modeling with a further challenge and a new set of interesting final channels [4].

Even when one limits the analysis to energies below the Ps formation and only studies elastic and inelastic (subreactive) processes, the use of positrons as projectiles is able to produce final cross sections that are markedly different from those observed and computed for electrons as projectiles and over a similar range of collision energies. Thus, it becomes important to be able to complement the increasing quality and variety of experimental data with a similar analysis from theoretical models and computational results.

Within a theoretical context, in fact, positrons represent on one hand simpler projectiles to handle from the point of view of their interactions with atomic and molecular systems, since the lack of the antisymmetry requirement for the total, fixed-nuclei (FN) wave functions eliminates the presence of nonlocal exchange interaction with the bound electrons. On the other hand, they also pose a different type of challenge when describing as best as possible the correlation and polarization effects coming from the response of the target electronic density to the perturbation from the impinging positrons. In this case, in fact, the repulsive nature of the

nuclear Coulomb forces tends to keep the low-energy positrons, in a classical sense, outside the short-range region of the molecular target and therefore, in the interaction, the dynamical correlation effects from the intermediate-range region are more important than the more conventional static correlation contributions as given by the well-known configuration interaction (CI) expansions [5]. This also means that the capability of the positrons to transfer their energy to internal nuclear degrees of freedom, e.g., to molecular rotations and vibrations, is going to be rather different from that of the electrons for similar molecules and for similar energies.

In the present study we therefore decided to carry out such an analysis for the CO₂ molecular target and to apply a computational scheme that we have already tested successfully for atomic targets [6,7] and for simpler molecular targets [8]. In particular, we analyze below the effect of various ways to model the short-range correlation forces and the long-range polarization forces on the final, elastic integral cross sections below the Ps formation threshold. We also analyze the elastic differential cross sections and both the integral and differential cross sections (DCS) for rotationally inelastic collisions. In the next section we briefly remind the reader of our theoretical model while in Sec. III we see the specific forms of the local correlation-polarization potentials employed for the CO₂ molecule. Section IV reports the elastic integral cross sections while Sec. V describes the rotationally inelastic processes. Our general conclusions are summarized in Sec. VI.

II. THE THEORETICAL MODEL

When discussing the quantum dynamics of positron collisions with molecular systems at energies below the threshold for positronium (Ps) formation one needs to know the following aspects of the whole process: (i) the anisotropic charge distribution of the molecular target and the corresponding static interaction of it with the e^+ projectile; (ii) the short-range and long-range correlation forces between the bound electrons of the target and the impinging positron; (iii)

*Author to whom correspondence should be addressed. FAX: +39-6-49913305. Electronic address: FAGIANT@CASPUR.IT

the actual couplings between the motion of the projectile within the interaction region and the nuclear degrees of freedom of the molecular target (rotations and vibrations). Each of the above ingredients obviously plays an important role in defining the size and behavior of the final total cross sections, integral and differential, and it is therefore important to realize that different levels of approximation for each of them have to be carefully compared and assessed. We will start by assuming the usual fixed-nuclei approximation (FNA), whereby the vibrational motion and the rotational degrees of freedom are factored out during the dynamics [8] and it is assumed that the corresponding cross sections can be obtained by considering the molecular geometry as both fixed in space and nonvibrating during the scattering time. A more detailed study on the vibrational-rotational motion and on its effect on total cross sections will be discussed elsewhere [9] but will be considered for the moment outside the scope of the present paper.

The first two points mentioned above, on the other hand, still need to be taken into account and we have carried out the actual evaluation of the static interaction $V_{st}(r_p)$, by expanding the self-consistent-field (SCF) wave function of the molecule at its equilibrium geometry R_{eq} around the molecular center of mass (CM)

$$V_{st}(r_p, \gamma; R_{eq}) = \sum_{\lambda=0}^{\lambda_{max}} V_{\lambda}^{st}(r_p; R_{eq}) P_{\lambda}(\cos \gamma), \quad (1)$$

where $\gamma = \arccos \hat{\mathbf{R}}_{eq} \cdot \hat{\mathbf{r}}_p$ within the body-fixed (BF) frame of reference with the molecular axis being chosen as the \hat{z} axis. In the present case the above expansion only involves even values of λ and the electronic wave function was expanded beforehand around the same CM, using a number of terms at least equal to λ_{max} , as we shall describe more extensively in the next section, while an even larger number of terms was used for the nuclear part of the static interaction. Below the threshold of Ps formation, the most serious of the questions about the above point (ii) concerns the clarification of the role played by long-range polarization forces and by short-range correlation effects: the models employed to treat positron scattering, in fact, turn out to yield final cross sections that are sensitive to the detailed handling of both the above contributions, especially at collision energies below a few eV [10,11].

The more direct numerical approach is to employ an extensive CI expansion of the target electronic wave function over a suitable set of excited electronic configurations and to implement it via Hylleraas-type functions that can describe the positron wave function within the molecular charge distribution [12]. On the other hand, such expansions are often very energy dependent and converge usually too slowly to be a useful tool for general implementation to complex molecular targets, where truncated expansions could be too small to be realistic [13]. As a consequence, there has been considerable interest in recent years in developing alternative treatments, which generate global modelings of correlation-polarization (CP) forces that do not depend on empirical parameters but can be implemented more easily via some simplified local representation of the $V_{CP}(\mathbf{r}_p)$ interactions [14–16].

The asymptotic expression for such a field is independent of the sign of the impinging charge and, for the simpler spherical component, is given by the well-known second-order perturbation expansion formula

$$V_{CP}^{\lambda=0}(r_p) \underset{r_p \rightarrow \infty}{\sim} V_{pol}^{(2)}(r_p) = \sum_{\ell=1}^{\infty} \frac{\alpha_{\ell} q^2}{2r_p^{2\ell+2}}, \quad (2)$$

where r_p represents the positron coordinate, q its charge, and the α_{ℓ} are the multipolar (here geometry-dependent) static polarizabilities of the target [17]. In most scattering treatments [18] only the lowest-order term is usually kept in the expansion (2), thereby viewing the distortion of the target electrons as chiefly resulting from the induced dipole that leads to the familiar r_p^{-4} asymptotic form of $V_{pol}^{(2)}$ with the molecular dipole polarizability α_D as its only coefficient in the sum on the right-hand side of Eq. (2).

The main drawback of this equation, however, is that it fails to correctly represent the true short-range behavior of the full interaction and does not contain any effect from both static and dynamical correlation contributions [19]. In order to correct for such failures we have proposed a while ago [20,21] the use of a local density functional approximation whereby the dynamic correlation effects that dominate the short-range behavior of the $V_{CP}(\mathbf{r}_p)$ for closed-shell molecular targets can be treated via a gradient-corrected density functional formula [22], which globally depends on the anisotropic charge density of this bound molecular electron. Such an approach, for the details of which we refer to our earlier papers [20,21], has turned out to work rather well for low-energy electron-molecule scattering processes [23,24] and has also provided good results for positron scattering from H_2 and N_2 molecules [8,9].

It is important to point out that the density-functional theory (DFT) formulation of the short-range correlation effects within the $V_{CP}(\mathbf{r}_p)$ is employed within the range of the target electronic density and produces an analytic expression in local form that is energy independent in terms of the scattering process. However, because of the special choice of the correlation factor f_c in the expression of the correlation energy [6], E_c is given by

$$E_c(N) = -\frac{1}{2} \int P_{HF}^{(2)}(\mathbf{r}, \mathbf{R}) f_c(\mathbf{r}, \mathbf{R}) \frac{d\mathbf{r} d\mathbf{R}}{2}, \quad (3)$$

one introduces implicitly nonadiabatic effects in the correlation energy [25]. Here $P_{HF}^{(2)}$ is the second-order Hartree-Fock density matrix without spin, $\mathbf{R} = \frac{1}{2}(\mathbf{r}_1 + \mathbf{r}_2)$, $\mathbf{r} = (\mathbf{r}_1 - \mathbf{r}_2)$, and $\mathbf{r}_1, \mathbf{r}_2$ refer to the coordinates of the correlated bound electrons. The factor $f_c(\mathbf{R}, \mathbf{r})$ deals with the dynamic correlation and assumes that, to begin with, the bound electron system is well described by a single determinant (SD), Hartree-Fock wave function. Furthermore, the DFT formulation for the above factor is equally applicable to electrons and positrons as perturbing projectiles since it deals solely with correlation effects caused by the N bound electrons at a given point in space

$$V_{CP}^{DFT}(\mathbf{r}_p) = \frac{\partial}{\partial \rho_N(\mathbf{r}_p)} E_c(\rho_N(\mathbf{r}_p)) \quad (4)$$

within the short-range (SR) interaction region.

Such a choice, on the other hand, implies that it is plausible to define a local functional form for the correlation potential without introducing the distinctions between the nonadiabatic effects that electrons and positrons have as projectiles on the target wave functions [26]. It will be shown below that in the present full formulation of the $V_{\text{CP}}(\mathbf{r}_p)$ interaction the long-range (LR) region is obtained rather simply by directly finding a specific radial value, r_c , outside of which the interaction is given by the V_{pol} expression of Eq. (2) for each of the contributing multipolar terms of Eq. (1). In other words, the present modeling of $V_{\text{CP}}(\mathbf{r}_p)$ over the whole range of action is obtained by the DFT formulation of Eq. (4) in the nonadiabatic SR region and by the lowest perturbative contributions to Eq. (2) in the LR region. Since this is done for each multipolar coefficient, different r_c^λ crossing radii are found depending on the functional form used for the f_c factor of Eq. (3) [8]. Since such choices turn out to be different for electrons and positrons [6], one may argue that the present model has a built-in way to correct for the necessary differences between e^+ and e^- as projectiles when describing SR correlation effects.

To give more specific examples of such differences we therefore discuss in the following section the possible choices for the positron interaction with the CO_2 molecule.

III. THE INTERACTION POTENTIAL

In the DFT formulation of the short-range correlation forces [21], the f_c factor in Eq. (4) requires the choice of an exponent, $\beta(\mathbf{r}_e)$, which is related to the excluded volume of the bound electron, V_{el} . The latter quantity describes that spatial region where the electron-electron (positron) correlation functions are appreciably different from zero and is related, in the DFT treatment, to the total electron density of the target system ρ :

$$V_{\text{el}} = 4\pi \int_0^\infty \exp(-\beta^2 r^2) r^2 dr = \frac{\pi^{3/2}}{\beta^3} = k\rho^{-1}. \quad (5)$$

Here k represents the average number of electrons within V_{el} [27]. One could therefore further write that

$$\beta(\mathbf{r}_{\text{el}}) = \frac{\pi^{1/2}}{k^{-1/3}\rho^{1/3}} = q\rho^{1/3}. \quad (6)$$

The factor q can now be obtained from the exact two-electron correlation energy in the He atom [28,22]. This choice will be described in our work as the Lee-Yang-Parr [22] (LYP) form of the $V_{\text{CP}}(\mathbf{r}_p)$ interaction. On the other hand, it was also suggested that it may be more realistic to select the correlation energy of the excited states of the same atomic system [29] and therefore a different value of the factor q could be obtained. Since we have also tried such a choice in the present calculations, we shall call it the Carravetta-Clementi [29] (CC) form of the $V_{\text{CP}}(\mathbf{r}_p)$ interaction.

A simpler approach to the evaluation of the short-range correlation effects, on the other hand, can also come from treating the impinging positron in the SR region as being immersed in a free-electron gas from the N bound electrons that can in turn provide a direct analytic form of the $V_{\text{CP}}(\mathbf{r}_p)$ interaction [15,23]. We shall call the latter option the FEG correlation-polarization potential. In the case of positron projectiles, it was further pointed out that the FEG formulation should be modified to account for the attractive static effects that the latter projectile experiences within the volume of the bound electrons [30,31] and therefore the FEG form can be further corrected into the positron correlation potential (PCOP) expression for the present $V_{\text{CP}}(\mathbf{r}_p)$ interaction. As we shall see below, a comparison of the relative shapes of such correlation-polarization potentials can indeed help us to see more clearly the most effective modeling of such forces for low-energy positron scattering off more complicated molecular targets. The resulting cross sections, and their comparison with the existing experiments, are in fact a rather sensitive test on the quality of such models.

The bound electron density for the ground state was obtained for a fixed nuclear geometry of $R_{\text{eq}} = 2.19440a_0$ and obtained from an SCF calculation over an extended set of Slater-type orbitals [32]. The total energy of -187.70366 eV was rather close to the Hartree-Fock (HF) limit. The further single-center expansion of the occupied molecular orbitals was carried out as described before [8] and the maximum value retained in the single-center expansion (SCE) evaluation was $l_{\text{max}} = 16$. The highest multipolar coefficient of Eq. (1) that was kept in the calculations was therefore $\lambda_{\text{max}} = 16$.

The long-range static contribution for $\lambda = 2$ yielded a value of the molecular quadrupole of $-3.63ea_0^2$, which compares well with the experimental value of $-3.908ea_0^2$. The values of the dipole polarizabilities that we employed in the potential of Eq. (2) were those given in Ref. [33]: $17.9a_0^3$ for α_0 and $9.19a_0^3$ for α_2 . These are the same values employed in a model calculation carried out earlier on positron- CO_2 scattering [34]. To make the comparison visually less difficult, we report in Fig. 1 only the lowest two coefficients of the expansion for the $V_{\text{CP}}(\mathbf{r}_p)$ interaction, i.e., the $\lambda = 0$ and $\lambda = 2$ coefficients of Eq. (1). In the upper part of the figure we show the spherical term, while the quadrupolar term is shown in the lower part of the same figure. The following comments could be readily made by examining the various forms of $V_{\text{CP}}(\mathbf{r}_p)$ potentials: (i) the r_c values of the innermost crossings between short-range correlation potentials and long-range polarization potentials are all very similar and are located around $4a_0$, in keeping with earlier values for polyatomic systems [35] interacting with electrons; (ii) the LYP and CC potentials from the gradient-corrected DFT formulation go rapidly to a ‘‘damped’’ finite value at the origin and are rather close to each other both in size and behavior and for both the $\lambda = 0$ and the $\lambda = 2$ contributions; (iii) the correlation-polarization models, which employ the simpler free-electron gas approach, the FEG and PCOP potentials, are both going to a finite value, as $r_p \rightarrow 0$, much more slowly than the former potentials. The PCOP is seen here to be by far the strongest correlation potential model in the inner region; (iv) the DFT modeling used here treats the

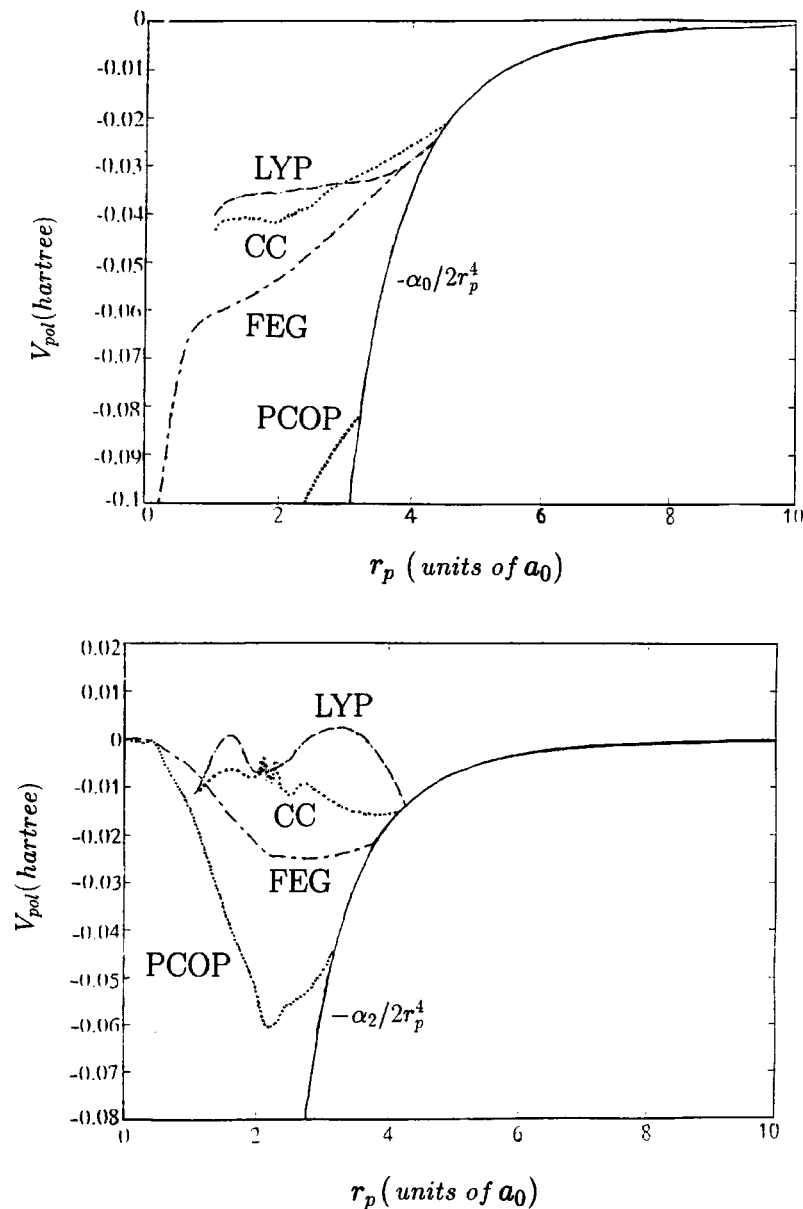


FIG. 1. Computed correlation-polarization potentials for the present system. Upper part, V_0 component of Eq. (1); lower part, V_2 component of Eq. (1). The labels of the DFT forms are discussed in the main text.

dynamic correlation effects from positrons in the same way as that for electrons, while the differences are introduced by different choices for the r_c values produced by long-range polarization [6], as we shall discuss below.

It is, in fact, important to note that the two forms of DFT correlation models differ in another aspect when combined with the long-range polarization potential. This is shown in Fig. 2, where both coefficients of Fig. 1 are reported on an enlarged energy scale. We see that the $\lambda=0$ components of the LYP and the CC forms show a similar inner crossing with the polarization potential around $4a_0$, but they also show secondary outer crossings that are, however, very different: the outer LYP value is around $5a_0$, i.e., not much different from the inner one, while the outer CC value has moved to about $8a_0$. The expanded exclusion volume of the CC form appears therefore to affect the strength of the dynamic correlation by making it larger, as r_p increases, than that from the LYP form. The same features are found for the $\lambda=2$ coefficients of the lower part in Fig. 2.

These differences of behavior can be seen, combined with

the stronger static interaction of the positron with the nuclei and the bound electrons, in the plots reported in Fig. 3. The lower part of the figure shows that the different choices for the correlation factor within the DFT formulation of the short-range correlation forces lead to fairly small differences between $V_{CP}(r_p)$ potentials. By selecting the inner cutoff into the polarization region the two models, in fact, show very similar forms for the lowest two multipolar coefficients of expansion (1), with the larger differences appearing in the anisotropic term. Thus, we expect that they will in turn affect little the behavior and values of the final cross sections.

The upper part of the same figure shows, for the LYP model, the effect of selecting the outer crossing of the DFT correlation potential into the polarization region of Eq. (2). For this specific form of $V_{CP}(r_p)$ we now find that the two crossing points are rather close to each other and make little difference in the strength of the spherical term. The anisotropic interaction, on the other hand, becomes stronger in the “well” region as expected from the behavior of Fig. 2. In other words, we see that the selection of either of the cross-

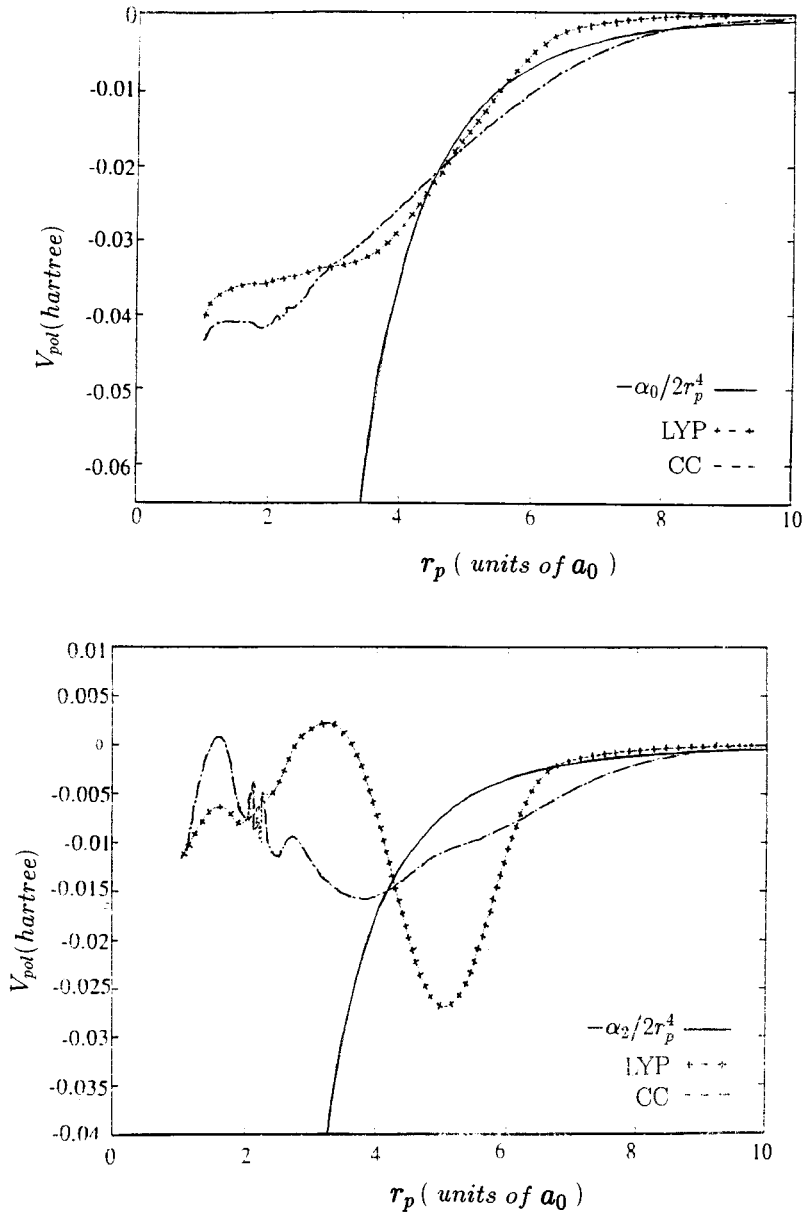


FIG. 2. Spherical and nonspherical components of the computed $V_{CP}(r_p)$, as discussed in the main text, for two different choices of the correlation factors: LYP from Ref. [22] and CC from Ref. [29].

ing radii (determined by the interplay between short-range DFT correlation and values of the molecular dipole polarizabilities) makes a difference in the angular strength of correlation and its effects on the final cross sections, as we shall see in the next section, can help us to better understand its role for positron projectiles as opposed to its effects for electron scattering processes, where the inner r_c values were always chosen [23,24].

IV. INTEGRAL AND DIFFERENTIAL CROSS SECTIONS

For nonpolar molecules the scattering of low-energy positrons from molecular targets can be treated within the familiar fixed-nuclei approximation even more safely than in the case of electron projectiles [36,37]. In this instance, in fact, to consider the rigid molecule as being fixed in space during the scattering process may be more valid at low collision energies than for electron projectiles since the latter penetrate more deeply into the molecular target charge distributions and therefore experience longer interaction times.

The FNA Hamiltonian is now invariant under the linear molecule rotations [18] and therefore the continuum solutions for each molecular geometry \mathbf{R} can be expanded over eigenfunctions of the \mathcal{L}^2 and \mathcal{L}_z angular momentum operators, at the chosen collision energy E , and the corresponding radial coefficients can be obtained [18] from the familiar set of coupled equations

$$\left\{ \frac{d^2}{dr_p^2} + \frac{\ell(\ell+1)}{2r_p^2} - (E - E_0) \right\} \mu_{\ell, \ell_0}^{E \wedge}(r_p) + \sum_{\ell'} V_{\ell \ell'}^{\wedge}(r_p | R) \mu_{\ell, \ell_0}^{E \wedge}(r_p) = 0, \quad (7)$$

where \wedge is the allowed eigenfunction of \mathcal{L}_z along the molecular bond axis for each ℓ value, E_0 is the reference energy equal to $k_0^2/2$, and E the actual collision energy. The corresponding coupling potential can be written as

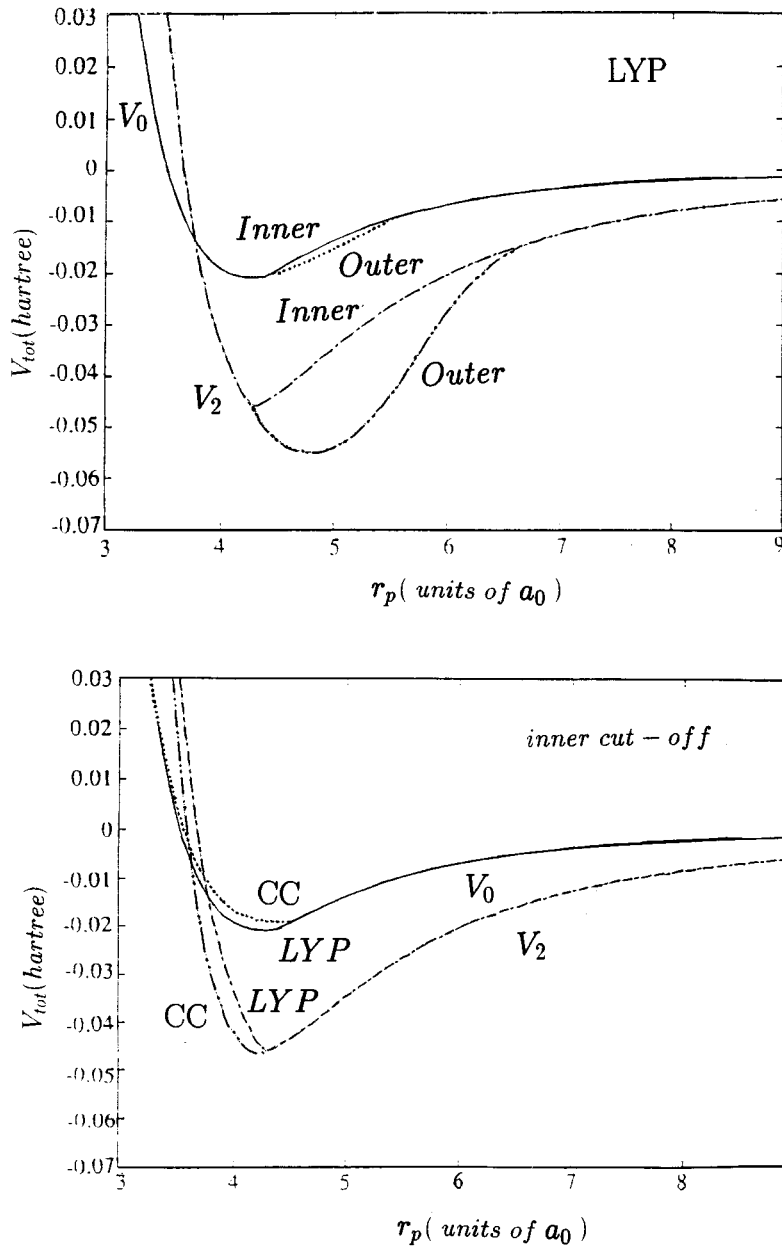


FIG. 3. Complete shape of the full interaction ($V_{st}+V_{CP}$) computed with the DFT model. Upper part, V_0 and V_2 components using the LYP form and two different crossing radii; lower part, comparison between LYP and CC forms.

$$V_{\ell\ell'}^{\wedge}(r_p|R) = \sum_{\lambda} V_{\lambda}(r_p;R) \times \int Y_{\ell'\ell}^*(\hat{r}_p) Y_{\lambda 0}(\hat{r}_p) Y_{\ell\ell}(\hat{r}_p) d\hat{r}_p, \quad (8)$$

where the coefficients outside the angular averaging are those discussed before and given by the expansion (1). From the usual boundary conditions imposed on the $\mu_{\ell\ell'}^{\wedge}(r_p)$ radial solutions [18] one recovers the BF T matrix, which is in turn related to the real R matrix by the usual expression

$$\underline{T} = [\underline{1} + \underline{R}][\underline{1} - i\underline{R}]^{-1}. \quad (9)$$

The solutions of the radial equation (7) are therefore searched for by solving the corresponding integral equations over the range of action of the potential, i.e., by integrating

out to $140a_0$ at the lowest energies and by numerically stabilizing the integral by testing several step choices [38]. In particular, we have employed Newton-Coates quadrature formulas in the region where all interaction is far from its asymptotic value while further on asymptotic forms were used for the lowest- λ coefficients (0 and 2). The higher values were given by fitting the static interaction to the usual multipolar forms

$$V_{\lambda}^{st}(r_p) = \frac{C_{\lambda}}{r_p^{\lambda+1}}. \quad (10)$$

Convergence of the final cross sections were tested by varying l_{\max} , λ_{\max} , and r_p^{\max} values. The set of values that gave the best converged results were $l_{\max}=20$, $\lambda_{\max}=16$, and $r_p^{\max}=140a_0$. The included \wedge contributions involved the Σ_g , Σ_u , Π_g , Π_u , Δ_g , and Δ_u components. No higher values of \wedge contributed significantly to the cross sections.

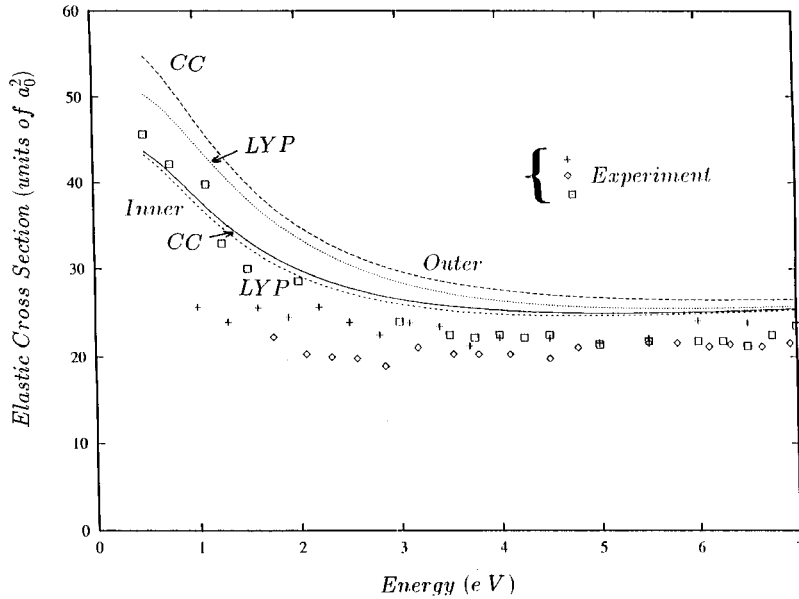


FIG. 4. Comparison between measured and computed elastic integral cross sections. The experiments are from Ref. [43] (+), Ref. [41] (□), and Ref. [42] (◇). The present calculations use the DFT forms from LYP and CC discussed in the main text.

The usual adiabatic nuclei-rotation (ANR) approach suggested long ago [39,40] evaluates the transition amplitude between initial and final rotational states of a linear rigid-rotor molecule, $\Gamma_i \equiv (j_i, m_i)$ and $\Gamma_f \equiv (j_f, m_f)$, from the quadrature

$$f_{\Gamma_i \Gamma_f}(\Omega' | E) = \langle \Gamma_f | f(\Omega', E | R, \beta) | \Gamma_i \rangle. \quad (11)$$

The solid angle Ω' defines here the direction of scattering in a space-fixed (SF) frame of reference and β labels the three Euler angles, $\beta \equiv (\alpha, \beta, \gamma)$, which specify the molecular orientation \hat{R} with respect to the space-fixed frame. Thus, the

scattering amplitude f within the quadrature of Eq. (11) refers also to a space-fixed reference frame but has been obtained from scattering parameters evaluated in the BF frame of reference [40]. The corresponding DCS can therefore be written as

$$\frac{d\sigma}{d\Omega}(j_i \rightarrow j_f) = \frac{k_{j_i, j_f}^{-2}}{4(2j_i + 1)} \sum_L A_L^{(j_i, j_f)}(E) P_L(\cos \vartheta), \quad (12)$$

where

$$\begin{aligned} A_L^{(j_i, j_f)}(E) &= (-)^L (2L+1)(2j_i+1)(2j_f+1) \sum_{\substack{\ell_i, \ell_f \\ \ell_i', \ell_f'}} (-)^{\lambda - \lambda'} i^{\ell_i - \ell_f - \ell_i' - \ell_f'} [(2\ell_i+1)(2\ell_f+1)(2\ell_i'+1)(2\ell_f'+1)]^{1/2} \\ &\times \begin{pmatrix} \ell_i & \ell_i' & L \\ 0 & 0 & 0 \end{pmatrix} \begin{pmatrix} \ell_f & \ell_f' & L \\ 0 & 0 & 0 \end{pmatrix} T_{\ell_i, \ell_f}^{\lambda} T_{\ell_i', \ell_f'}^{*\lambda} \sum_n (-)^n (2n+1) \begin{pmatrix} j_i & j_f & n \\ 0 & 0 & 0 \end{pmatrix}^2 \begin{pmatrix} \ell_i & \ell_f & n \\ \lambda & -\lambda & 0 \end{pmatrix} \\ &\times \begin{pmatrix} \ell_i' & \ell_f' & n \\ \lambda' & -\lambda' & 0 \end{pmatrix} \begin{Bmatrix} \ell_i & \ell_i' & L \\ \ell_f' & \ell_f & n \end{Bmatrix}. \end{aligned} \quad (13)$$

The 3- j , 6- j , and 9- j coefficients have the usual meaning [18] and the T -matrix elements are those evaluated in the BF frame of reference by solving the set of coupled equations (7). Another quantity of interest related to the above DCS is the momentum-transfer cross section given by the following expression (in the FNA approximation)

$$\sigma_m(E) = \int \frac{d\sigma}{d\Omega} (1 - \cos \vartheta) d\Omega. \quad (14)$$

The computed elastic integral cross sections (rotationally summed) are then obtained directly from the BF T -matrix calculations [18] of Eq. (9) and are shown in Fig. 4 in comparison with various experimental data. What is shown there is the result of the present calculations carried out using different forms of the correlation part for the modeling of the $V_{CP}(\mathbf{r}_p)$ interaction in the scattering problem. Thus, CC labels the DFT calculations using one type of correlation factor in Eq. (6) [29], while LYP uses the same factor as that

employed in Ref. [22]. At the same time, the curves labeled “inner” refer to the smaller values of r_c that connect the correlation potential with the LR dipole polarization interaction, while those labeled “outer” use the larger r_c values for this connection. We see that the differences between the LYP and CC models of correlation factors play a rather small role compared with the selection of a different r_c value: the latter choice invariably produces larger correlation effects, especially at the lower collision energies.

Thus, considering the rather large spread of the available experimental points [41–43] one can conclude that the present calculations reproduce at best the measured values when using the LYP correlation potential and its inner radial connection values with the long-range dipole polarization forces. Interestingly enough, this was also the result found for electron scattering from similar targets [4], where only the weaker correlation-polarization potential was deemed to be more realistic.

A further comparison with experiments of the computed elastic (rotationally summed) integral cross sections is shown in Fig. 5, where we also report the results obtained using the DFT model in its simpler version of a free-electron-gas expression for the correlation-polarization potential: the FEG calculations use the analytic form applicable to electrons [15] while the PCOP calculations include the local correction for a positron as a perturbing projectile [30,31]. Finally the earlier calculations of Ref. [34] are also reported and labeled “Darewych” in the figure. They correspond to FNA calculations in the BF frame of reference using a parametric cutoff of the polarization potential, adjusted to give agreement with measurements at 5 eV. We see the following from the shown comparison. (i) As expected the LYP, FEG, and PCOP behave similarly at low collision energies, where the polarization part of the V_{CP} potential dominates but differ as the collision energy increases because the short-range part of the correlation becomes more important during collisions. (ii) The LYP and FEG formulations produce very similar results over the whole range of energies in spite of their different shapes at short distances seen in Fig. 1. Obviously such differences are made less important by the dominant static interaction, while the fact that both potentials show a

similar value of r_c is causing the behavior of the scattering cross sections to remain essentially the same. (iii) The PCOP potential within the free-electron-gas model produces the smallest cross sections, in agreement only with the experiments of Ref. [42] but markedly smaller than those from Refs. [41] and [43]. This is at variance with the earlier results for atomic systems [6], where the integral cross sections that were obtained from the PCOP model potentials were much larger than the other cross sections at all energies below Ps formation. It is worth noting, however, that all the DFT calculations shown here are to our knowledge the first attempt to compute cross sections from e^+ scattering from CO_2 since the earlier empirical model of Ref. [34] was employed. The present results clearly indicate, as already seen for H_2 and N_2 , that this modeling of the V_{CP} interaction without any adjustment to experiments produces a rather good description of the short-range correlation forces with a very limited computational cost. It therefore becomes useful to extend their use to the evaluation of the ANR differential cross sections following Eq. (12) and over the same range of collision energies examined by the FNA integral cross sections.

The results reported in Fig. 6 show, in the upper part of the figure, the behavior of the rotationally summed angular distributions as a function of collision energy, going from 1 up to 7 eV across the range examined by the integral cross sections of Figs. 4 and 5. We clearly see from the calculations that the forward scattering region dominates at the lower collision energies where our results suggest the first few only scattering angles to be relevant for maximum positron flux. On the other hand, as the collision energy increases and the projectile samples the inner region of the interaction we see that the maximum scattered flux moves now at larger scattering angles, thus making its detection experimentally easier in a different range of angular distributions.

V. ROTATIONALLY INELASTIC COLLISIONS

It is well known that the natural extension of FNA calculations to what is called the ANR approximation [44,45] merely implies a transformation from a body to a space

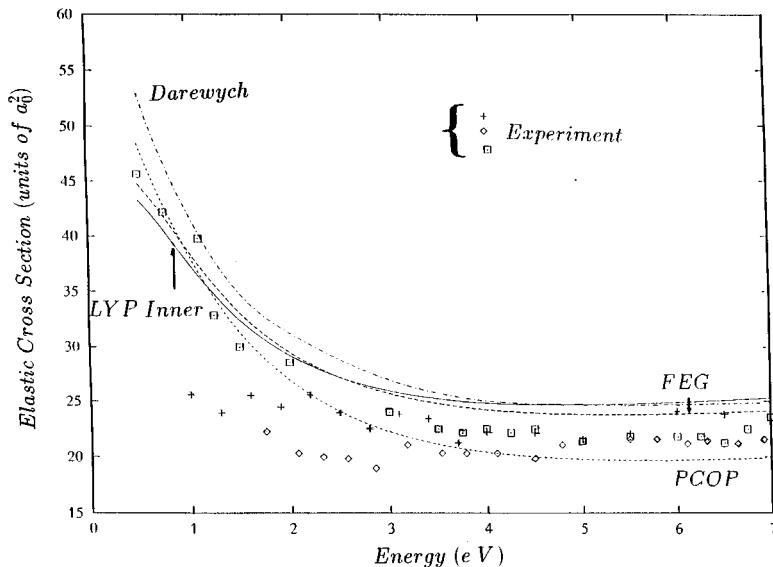


FIG. 5. Comparison of measured and computed elastic integral cross sections. The calculations are Darewych, from Ref. [34]; LYP, present results with correlation form of Ref. [22]; FEG, present results with correlation form of Ref. [15]; and PCOP, present results with correlation form of Ref. [31]. The experiments are the same as in Fig. 4.

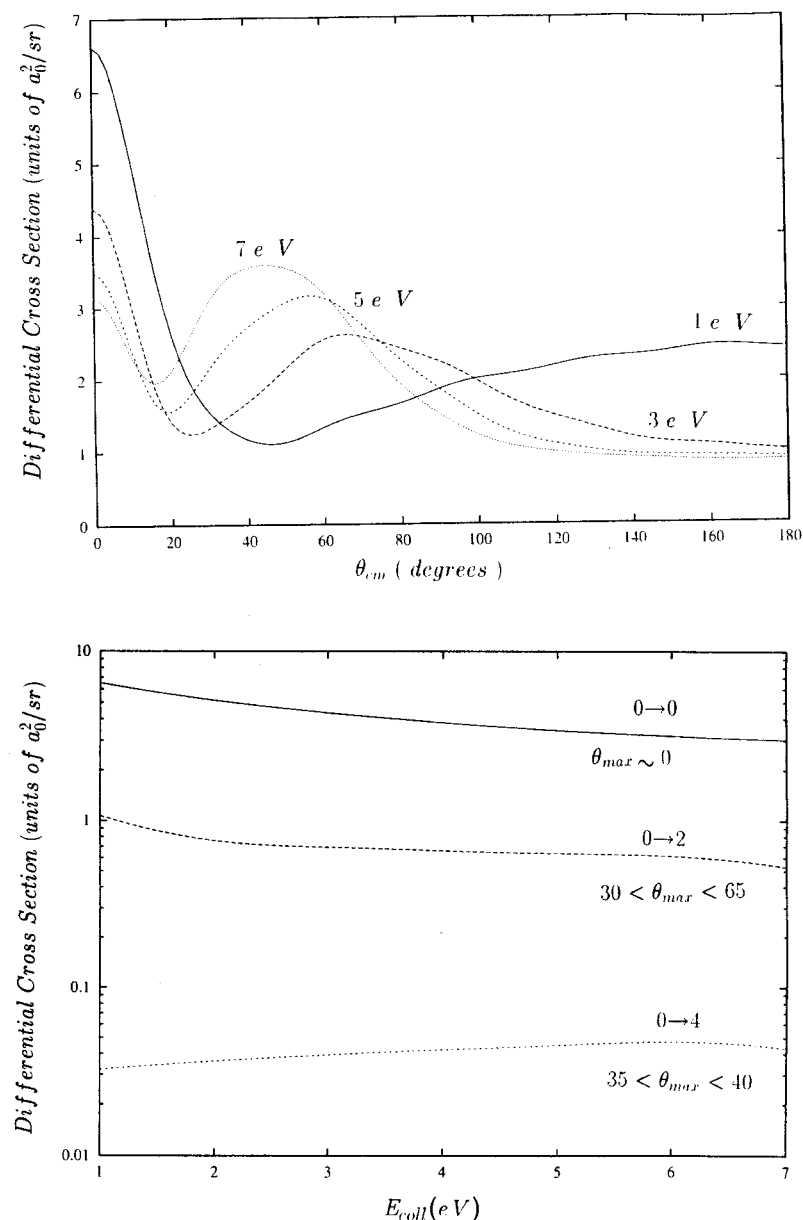


FIG. 6. Computed differential cross sections (DCS) at different collision energy. LYP form of correlation potential. Lower part: maximum values of partial DCS in the stated angular range and as function of collision energy.

frame of reference without changing the dynamics of the collision problem. Thus, if the physical approximation of an interaction time τ shorter than the rotational time t_r is valid at the considered energies, then one can simply use for the state-to-state differential cross sections associated to rotational excitations the expression given by Eq. (12) in which the BF-FNA results for the T matrix are transformed via the SF-ANR approximation [45]. Thereby making the $A_L^{(jj')}$ coefficients now dependent on the initial and final rotational states of the target through the SF T -matrix elements that appear in it and that come from a simple geometrical (BF \rightarrow SF) transformation [40,46].

Examples of such partial differential cross sections are shown in Fig. 7 at two different collision energies: at 1 eV (upper part of the figure) and at 5 eV (lower part of the figure). The range of intensity values is so large that they are presented on a logarithmic scale for transitions involving excitations from the ground rotational level. We can readily notice the following points. (i) The inelastic transitions, at the lower collision energies, are not showing the forward

scattering features observed before in the total DCS. On the other hand, the $(0 \rightarrow 0)$ cross sections show here a strong forward peak, which also persists at the higher collision energy (lower diagrams in Fig. 7). Thus, we can see that any low-energy forward scattering mostly comes from the elastic component. (ii) Of the inelastic processes, the $(0 \rightarrow 2)$ excitation is the only one that is comparable in size with the elastic DCS: all other excitations with higher Δ_j transitions are much smaller by various orders of magnitudes. This feature persists even at the higher collision energies. We can therefore say that rotational excitation by positron scattering is a rather inefficient process due to the little penetration (perturbation) caused by the latter projectile into the molecular volume.

The dependence of the partial cross section maximum value on the chosen collision energy could be seen more clearly in the lower part of Fig. 6. We report there, as a function of collision energy, the maximum values of the state-to-state DCS in order to indicate which deflection angles would be more amenable to detection. Thus, the elas-

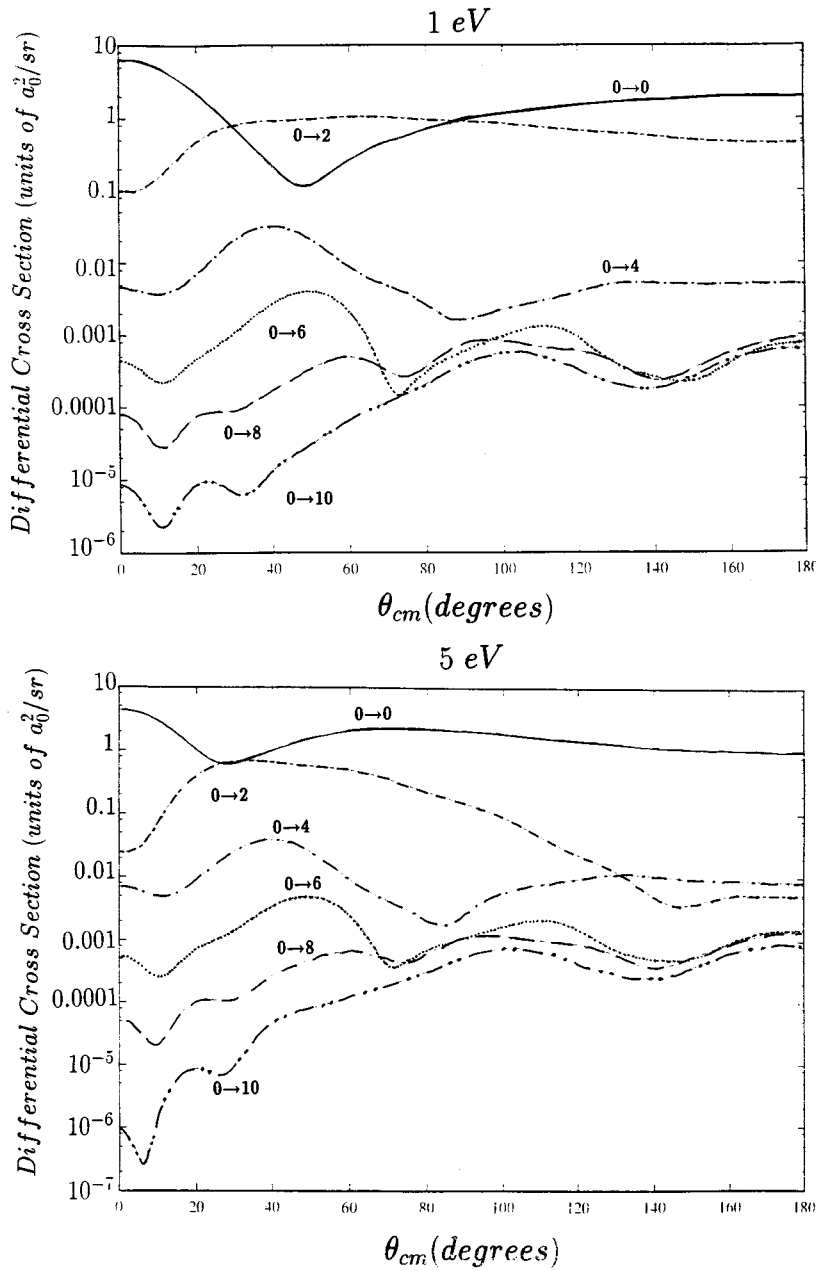


FIG. 7. Partial elastic and inelastic DCS computed at two different collision energies: upper part, at 1 eV; lower part, at 5 eV. LYP correlation and ANR dynamics.

tic DCS maxima are seen to always peak in the forward direction over the whole range of examined energies. The inelastic DCS, on the other hand, are localized within a more narrow angular cone of “maximum flux” over the whole energy range. Thus, the inelastic maxima now vary only by about 2 orders of magnitude from the elastic DCS and may be more amenable to detection within each particular angular range.

From the previous equation we know that the corresponding state-to-state integral partial cross sections can be obtained as [46]

$$\sigma_{j \rightarrow j'}(E) = \frac{\pi k_j^{-2}}{2j+1} A_0^{(j,j')} \quad (15)$$

$$= \frac{\pi k_j^{-2}}{2j+1} \sum_{J, J'} (2J+1) |T_{j' \ell', j, \ell}^J|^2, \quad (16)$$

where the T -matrix elements are now given in the SF frame of reference [47]. The corresponding momentum transfer quantities are also obtained in terms of the A_L coefficients:

$$\sigma_{j \rightarrow j'}^m(E) = \frac{\pi k_j^{-2}}{2j+1} \left[A_0^{(j,j')} - \frac{1}{3} A_1^{(j,j')} \right] \quad (17)$$

and can be readily computed from the ANR transformation discussed before. Both the above quantities will be a measure of the general efficiency of positron projectiles in bringing about the rotational excitation of the CO_2 target.

In the upper part of Fig. 8 we therefore report the energy dependence of the partial integral cross sections for the elastic and the two largest inelastic excitation processes, ($0 \rightarrow 2$) and ($0 \rightarrow 4$). We see that the elastic process clearly dominates the collisional encounters, with the lowest two excitations being 1 and 2 orders of magnitude smaller. Fur-

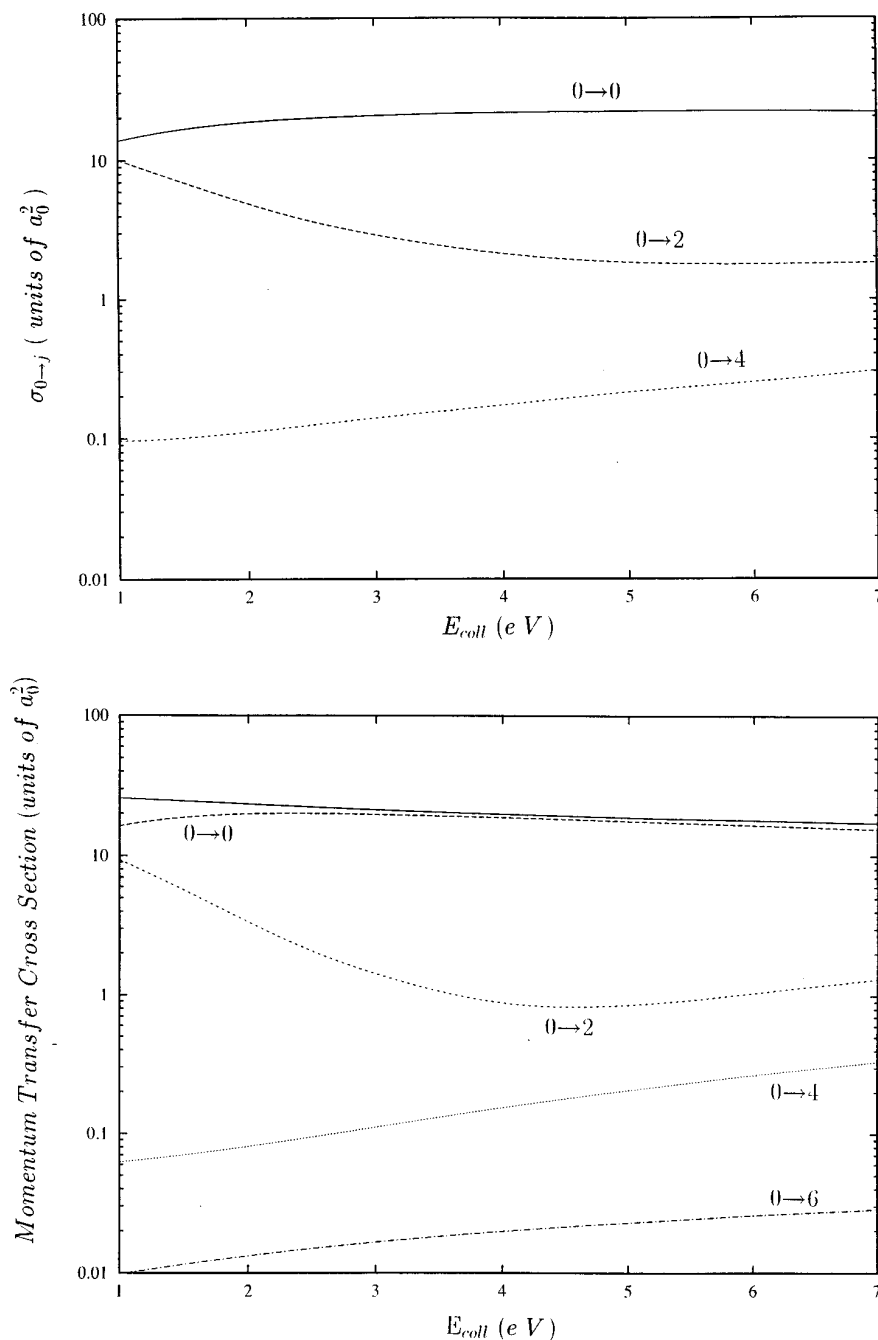


FIG. 8. Partial integral cross sections as a function of collision energy. Upper part, elastic and two inelastic contributions from Eq. (15); lower part, same for the momentum transfer cross sections. The total σ_m at Eq. (14) is shown by the solid line.

thermore, their energy dependence within the observed interval appear to be rather weak and show an increase of larger Δ_j inelasticity as E increases.

The same general behavior is shown by the $\sigma_{j \rightarrow j'}^m$, reported in the lower part of Fig. 8. The solid line shows also the total σ_m of Eq. (14), which clearly appears to nearly coincide with the elastic cross section. Here again one sees that the inelastic contributions increase with increasing collision energy.

A more expanded view of the behavior of the inelastic cross sections could be had by the calculations shown in Fig. 9. The upper part of the figure reports, at different collision energies, the values of the inelastic cross sections with Δ_j values up to 12, i.e., with very large values of energy transferred during collisions. As expected, such cross sections

span 4 orders of magnitude and are at all energies much smaller than the elastic process. Thus, if one now defines the average energy transfer in rotational excitation processes as given by

$$\langle E_{\text{rot}} \rangle_0 = \frac{\sum_{j'=0}^{j_{\text{max}}} \sigma_{0 \rightarrow j'} \Delta E_{0j'}}{\sum_{j'=0}^{j_{\text{max}}} \sigma_{0 \rightarrow j'}} \quad (18)$$

for collisional heating of the molecules out of the $j=0$ level, one can represent the above quantity as a function of collision energy to get some idea about the efficiency of the collisional excitation. The results from the present calculations

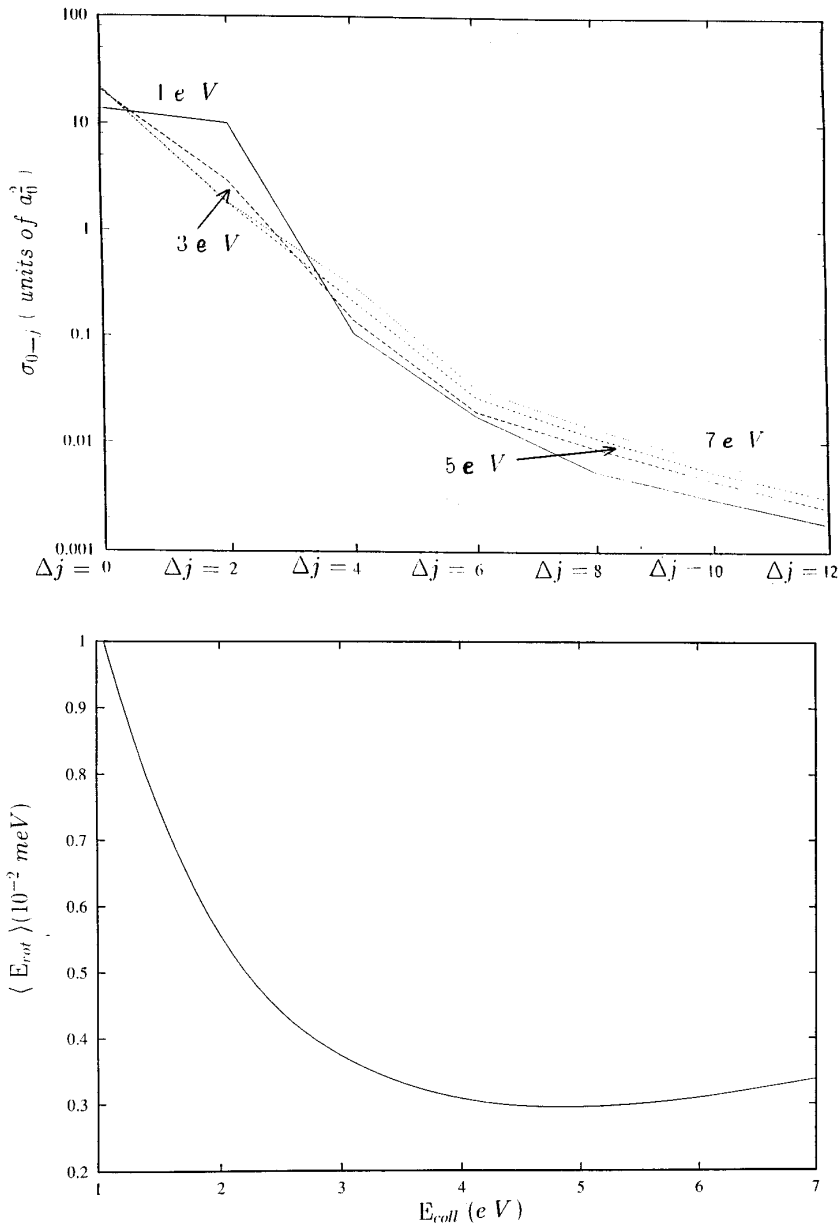


FIG. 9. Upper panel, partial integral inelastic cross sections at different collision energies and as a function of Δ_j transitions; lower panel, average computed energy transfer as a function of collision energy.

are shown in the lower part of Fig. 9, where the $\langle E_{rot} \rangle$ values as plotted over the range of energy below the Ps threshold. One clearly sees there that the amount of energy being transferred is really very small and drops very rapidly, because of the increase with E of the elastic process, in the low-energy range while slowly increasing as E reaches the 7-eV threshold. In other words, the positron projectiles are indeed far less efficient than electrons for the excitation of rotational levels in this system since the latter projectile shows much larger values of such cross sections at the same energies and indicates the strong influence of the resonant processes [48] in producing inelastic probabilities.

VI. SUMMARY AND CONCLUSIONS

In the present work we have reported a detailed study on the collision of low-energy positrons (below the threshold of Ps formation) with a linear polyatomic target, the CO_2 mol-

ecule. The computational approach has been that of using an *ab initio*, nonempirical modeling of correlation-polarization forces and of treating both the FNA and ANR dynamics within a single-center-expansion development. The results of the present calculations show the following. (i) The elastic integral cross sections (rotationally summed) agree rather well with available experiments and suggest that the DFT modeling of correlation forces provide, with a limited computational effort, a realistic description of the scattering process. (ii) The nature of the positron-molecule static interaction is such that the SCE expansion yields converged cross sections more rapidly than in the case of electron scattering with the same system [49]. (iii) The angular distributions are dominated by the forward-scattering elastic component, while inelastic DCS show maximum values only within limited angular cones away from the small- ϑ region. (iv) The size of the inelastic cross sections is generally very small and strongly decreases with increasing energy transfer, thus indicating that positrons are much less efficient projectiles than

electrons at the same collision energies [48], in producing molecular heating in the gas.

In conclusion, we have presented a more detailed picture of both elastic and inelastic collisions at low energies of positrons with a polyatomic target. In this picture the present interaction model appears to yield results that are in reasonably good accord with the available experiments. The extension of the ANR approach to vibrationally inelastic processes

is presently under study and will be discussed elsewhere [50].

ACKNOWLEDGMENTS

The financial support of the Italian National Research Council (CNR), of the Italian Ministry for University and Research (MURST), and of the Research funds from the University of Rome are gratefully acknowledged.

-
- [1] *Positron Interactions with Atoms, Molecules and Clusters* (J. C. Baltzer AC, Science Publishers, Singapore, 1994).
- [2] *Positron (Electron) Gas Scattering*, edited by W. E. Kauppila, T. S. Stein, and J. M. Wadhera (World Scientific, Singapore, 1986).
- [3] *Electron Collisions with Molecules, Clusters and Surfaces*, edited by H. Ehrhardt and L. A. Morgan (Plenum, New York, 1994).
- [4] For example, see F. A. Gianturco and R. Melissa, *Europhys. Lett.* **33**, 661 (1996).
- [5] H. D. Meyer, *J. Phys. B* **25**, 2657 (1992).
- [6] F. A. Gianturco, A. Jain, and J. A. Rodriguez-Ruiz, *Phys. Rev. A* **48**, 4321 (1993).
- [7] F. A. Gianturco and D. De Fazio, *Phys. Rev. A* **50**, 4819 (1994).
- [8] A. Temkin and K. Vasavada, *Phys. Rev.* **160**, 109 (1967); F. A. Gianturco, P. Paoletti, and J. A. Rodriguez-Ruiz, *Z. Phys. D* **36**, 51 (1995).
- [9] F. A. Gianturco and T. Mukherjee, *Phys. Rev. A* **55**, 1044 (1997).
- [10] M. A. Morrison, *Phys. Rev. A* **25**, 1445 (1982).
- [11] T. L. Gibson, *J. Phys. B* **23**, 767 (1990).
- [12] For example, see E. A. G. Armour, *Phys. Rep.* **169**, 1 (1988).
- [13] R. N. Hewitt, C. J. Noble, and B. H. Bransden, *J. Phys. B* **25**, 557 (1992).
- [14] M. A. Morrison, *Adv. At. Mol. Phys.* **24**, 51 (1988).
- [15] J. K. O'Connell and N. F. Lane, *Phys. Rev. A* **27**, 1893 (1983).
- [16] F. A. Gianturco and D. De Fazio, *Phys. Rev. A* **50**, 4819 (1994).
- [17] For example, see A. D. Buckingham, *Adv. Chem. Phys.* **12**, 107 (1967).
- [18] N. F. Lane, *Rev. Mod. Phys.* **52**, 29 (1980).
- [19] H. D. Meyer, *Phys. Rev. A* **40**, 5605 (1989).
- [20] F. A. Gianturco and J. A. Rodriguez-Ruiz, *Phys. Rev. A* **47**, 1075 (1993).
- [21] F. A. Gianturco and J. A. Rodriguez-Ruiz, *J. Mol. Struct.* **26**, 99 (1992).
- [22] C. Lee, W. Yang, and R. G. Parr, *Phys. Rev. B* **37**, 785 (1988).
- [23] F. A. Gianturco, N. Sanna, and J. A. Rodriguez-Ruiz, *Phys. Rev. A* **52**, 1257 (1995).
- [24] F. A. Gianturco and N. Stoecklin, *J. Phys. B* **27**, 5903 (1994).
- [25] R. Colle and O. Salvetti, *Theor. Chim. Acta* **37**, 329 (1975).
- [26] M. Morrison, in *Positron (Electron) Gas Scattering* (Ref. [2]), p. 100.
- [27] E. P. Wigner and F. Seitz, *Phys. Rev.* **43**, 804 (1933).
- [28] R. Colle and O. Salvetti, *J. Chem. Phys.* **93**, 534 (1990).
- [29] V. Carravetta and E. Clementi, *J. Chem. Phys.* **81**, 2646 (1984).
- [30] E. Boronski and R. M. Nieminen, *Phys. Rev. B* **34**, 3820 (1986).
- [31] A. Jain, *Phys. Rev. A* **41**, 2437 (1991).
- [32] A. D. Mc Lean and M. Yoshimine, *IBM J. Res. Dev.* **12**, 206 (1968).
- [33] M. A. Morrison, N. F. Lane, and L. A. Collins, *Phys. Rev. A* **15**, 2186 (1977).
- [34] M. Horbatsch and J. W. Darewych, *J. Phys. B* **16**, 4059 (1983).
- [35] F. A. Gianturco, *Europhys. Lett.* **12**, 689 (1990).
- [36] A. Jain and F. A. Gianturco, *Phys. Rev. B* **24**, 2387 (1991).
- [37] T. L. Gibson and M. A. Morrison, *Phys. Rev. A* **29**, 2497 (1984).
- [38] W. N. Sams and D. J. Kouri, *J. Chem. Phys.* **51**, 4809 (1969).
- [39] A. Temkin and K. V. Vasavada, *Phys. Rev.* **160**, 109 (1967).
- [40] A. Temkin and F. H. M. Faisal, *Phys. Rev. A* **3**, 520 (1971).
- [41] K. R. Hoffmann, M. S. Dababneh, Y.-F. Hsieh, W. E. Kauppila, V. Pol, J. H. Smart, and T. S. Stein, *Phys. Rev. A* **25**, 1393 (1982).
- [42] M. Charlton, T. C. Griffith, G. R. Heyland, and G. L. Wright, *J. Phys. B* **16**, 323 (1983).
- [43] O. Sueoka and S. Mori, *J. Phys. Soc. Jpn.* **53**, 2492 (1984).
- [44] F. A. Gianturco, A. Jain, and L. C. Pantano, *J. Phys. B* **20**, 571 (1986).
- [45] D. M. Chase, *Phys. Rev.* **104**, 838 (1956).
- [46] N. Chandra, *Phys. Rev. A* **16**, 80 (1977).
- [47] A. M. Arthurs and A. Dalgarno, *Proc. R. Soc. London A* **256**, 540 (1960).
- [48] F. A. Gianturco and T. Stoecklin, *Phys. Rev. A* **55**, 1937 (1997).
- [49] F. A. Gianturco and T. Stoecklin, *J. Phys. B* **29**, 3933 (1996).
- [50] F. A. Gianturco and T. Mukherjee, *Phys. Rev. A* (to be published).